Effect of Heat Treatment on Structural and Magnetic Properties of Li-Ni Ferrite Prepared via Sol-Gel Auto-Combustion Method

Jiali Song
Tianjin University
Zhi Wang (zhiwang@tju.edu.cn)
Tianjin University https://orcid.org/0000-0002-7058-0683
Yu Gao
Ningbo Institute of Materials Technology and Engineering CAS: Ningbo Institute of Industrial Technology Chinese Academy of Sciences

Original Research

Keywords: Annealing temperature, Cation occupation, Microstructure, Sol-gel method, Magnetic properties

Posted Date: February 4th, 2021

DOI: https://doi.org/10.21203/rs.3.rs-166543/v1

Effect of heat treatment on structural and magnetic properties of Li-Ni ferrite prepared via sol-gel auto-combustion method

Jiali Song[1], Zhi Wang[1,*], Yu Gao[2]

[1]School of Science, Tianjin University, Tianjin 300072, P. R. China
[2] Zhejiang Province Key Laboratory of Magnetic Materials and Application Technology, CAS Key Laboratory of Magnetic Materials and Devices, Ningbo Institute of Materials Technology & Engineering, Chinese Academy of Sciences, Ningbo, Zhejiang, 315201, China

[*] Corresponding author: Zhi Wang

Tel: +86-22-87892075; Fax: +86-22-27890681; E-mail address: zhiwang@tju.edu.cn

Abstract

Nanocrystalline $Li_{0.35}Ni_{0.3}Fe_{2.35}O_4$ ferrites were prepared at different annealing temperature by sol-gel auto-combustion method. The effects of the annealing temperature on the structure and magnetic properties of the synthesized Li-Ni ferrites were characterized by X-ray diffraction (XRD), scanning electron microscopy (SEM), Fourier transform infrared spectra (FT-IR) and Squid-VSM. Rietveld refinement of the X-ray diffraction data confirmed the occurrence of phase transition from α-spinel to β-spinel, from which the ideal cation occupation and lattice parameter can be obtained. The grain size increased significantly with annealing temperature. The variation of saturation magnetization can be well explained in terms of the occupation of ions in tetrahedron and octahedron. The coercivity initially increased and later decreased significantly from 115 to 37 Oe with the increase of annealed temperature which could be attributed the fact that the 600℃-annealed grain size is close to transition size from single to multidomain region.

Keywords: Annealing temperature; Cation occupation; Microstructure; Sol-gel method; Magnetic properties

1. Introduction

Nanocrystalline ferrites possess many excellent properties such as high electrical

resistivity, saturation magnetization and initial permeability. All these excellent properties make nanocrystalline ferrites show bright future in commercially significant in various applications and play a vital role in almost every field of technology, such as isolators, phase shifters, memory core and high-speed digital tapes etc.[1,2].To obtain efficient magnetic materials for application, the electric and magnetic properties of ferrites can be modified by changing the occupation of magnetic or non-magnetic cation in the spinel structure[3,4].

Recently, because of the excellent magnetic and electrical properties such as high Curie temperature, squareness of hysteresis loop, high and wide range of saturation magnetization, low dielectric and magnetic losses etc.[5–7], nanocrystalline lithium ferrites and substituted lithium ferrites have attracted considerable attention and replaced expensive magnetic garnets and other ferrites gradually. Wherein, the nanocrystalline Li-Ni ferrites have excellent performance in microwave applications due to their high resistivity, low eddy current losses, high Curie temperature and magnetic properties[8,9]. However, the performance of nano-scale ferrites is also more sensitive to the effects of chemical composition, preparation methods, sintering temperature, and sintering time, etc[10,11]. There are multiple synthesis method to prepare the Li-Ni ferrite systems, such as hydrothermal, high temperature ceramic technique, co-precipitation, sol-gel etc[12–16]. In the above preparation methods, sol-gel auto-combustion method can prepare ultra-fine crystalline powders exhibiting chemically homogeneous composition, uniform size and good reactivity. The advantages of this method are processing simplicity, low energy loss, high production efficiency and high-purity products[17–19]. It was reported that the high sintering temperature above 1050 °C will lead to the volatilization of lithium and oxygen and change of stoichiometry for the lithium ferrite, which will cause the deterioration of the magnetic and electric properties[20,21]. These facts motivated the authors to synthesize Li-Ni ferrites by the sol-gel auto-combustion method with low annealing temperature. In present study, we report the structural and magnetic properties of the $Li_{0.35}Ni_{0.3}Fe_{2.35}O_4$ samples with annealing temperature (Ta) from 500 to 850 ℃.

2. Experiment

The ferrites with composition of $Li_{0.35}Ni_{0.3}Fe_{2.35}O_4$ were prepared by sol-gel auto-

combustion method and annealed at temperature (Ta) of 500 ℃, 600 ℃, 700 ℃, 800 ℃ and 850 ℃ respectively. The stoichiometric amounts of analytical grade lithium nitrate [$LiNO_3$], nickel nitrate [$Ni(NO_3)_2 \cdot 6H_2O$], iron nitrate [$Fe(NO_3)_3 \cdot 9H_2O$] and citric acid [$C_6H_8O_7 \cdot H_2O$] were weighed according to the designed composition. The ratio of metal ions to citric acid is 1:1. Stoichiometric amounts metal nitrate and citric acid were dissolved in deionized water to form an aqueous solution. The pH of the resulting solution was adjusted to 6 by aqueous ammonia. Then the solution was heated at 80 ℃ for 2 hours to be viscous liquid with continuously stirring. The obtained sol was dried at 180 ℃ until burning to dendritic ash flakes. Then the burned ashes were grinded to a very fine powder using a glass mortar and pestle. The grinded powders were subsequently annealed at 500 - 850 ℃ for 4 h in a muffle furnace with a fixed heating rate of 5℃/min and then cooled to room temperature naturally. Finally, the powder samples were used for structural and magnetic measurements.

The phase identification of annealed powders was characterized by a D/MAX-2500 X-ray diffraction (XRD) using Cu Kα radiation (λ = 1.5405 Å). The Nanosem 430 field emission scanning electron microscopy (FESEM) examination was carried out to analyze the surface morphology of the annealed powders. Rietveld's refinements of all the samples were carried out using HighScore X′Pert Plus and Fullprof softwares. Fourier transform infrared spectra (FTIR) analysis was performed on a BIO-RAD FTS3000 IR spectra scanner. Magnetic behaviors of the samples were determined using a Vibrating Sample Magnetometer (VSM) at room temperature.

3. Results and Discussions

3.1 XRD analysis

Fig. 1 represents the Rietveld refined XRD patterns of $Li_{0.35}Ni_{0.3}Fe_{2.35}O_4$ powders annealed at 500 - 850 ℃. All the parameters collected through the refinement including Profile factor (R_p), weighted profile factor (R_{wp}), expected R-factor (R_{exp}), and reliability factors ($\chi^2 = (R_{wp}/R_{exp})^2$) are presented in Table 1. The lower Rp and χ^2 indicate the goodness of the refined XRD patterns. It is evident that the negligible difference between observed and calculated data indicate an extreme accuracy of calculated data. It is well

known that Lithium ferrite, $(Fe_1)_A[Li_{0.5}Fe_{1.5}]_BO_4$, displays an inverse spinel structure with Fe at tetrahedral 8a positions and a 1:3 mixture of Li and Fe at octahedral 16d positions. The latter are 16d Wyckoff's positions for disordered (*Fd*-3*m*) form, and 4b + 12d for the ordered ($P4_132/P4_332$) form[22]. From the figure 1, it is clearly seen that the appearance of additional reflections (210 and 211) on the X-ray diffraction patterns of (a) and (b) show that the ferrites annealed at 500 ℃ and 600 ℃ have α-phase spinel structure belonging to the space group $P4_332$ with order forms. And structure parameters of Specific occupation of ions annealed at 500 ℃ and 600 ℃ observed from refinement results are given in Table 2. It can be noticed that Li^+ ions only occupy octahedral 4b position, Ni^{2+} ions occupy at octahedral 4b and 12d sites in 1:1 ratio for the sample annealed at 500 ℃. As the temperature increases, a small amount of Ni^{2+} ions transfer from octahedron to tetrahedron. The compositions of ferrites with the ideal cation occupancy values, lattice parameter obtained by averaging the higher-order peaks are tabulated in Table 3. The increase of lattice parameter with annealing temperature below 600 ℃ can be attributed to the larger Ni^{2+} ions (0.55 Å) in place of smaller Fe^{3+} ions (0.49 Å) at tetrahedron. For the samples annealed above 600 ℃, the spinel phases have β-phase spinel structure belonging to space group *Fd*-3*m* in disordered forms. It is found that Ni^{2+} and Li^+ ions mainly occupy the octahedral position, and a few of them migrate to the tetrahedron position. A small amount of Ni^{2+} (0.55 Å) and Li^+ (0.59 Å) ions substitute Fe^{3+} (0.49 Å) in the tetrahedron, which results in the increase of lattice parameters. It is evident that the annealing temperature can result in the order-disorder transition of the $Li_{0.35}Ni_{0.3}Fe_{2.35}O_4$ ferrites analyzed by the Rietveld structure refinement method. The crystallite size (*D*) was calculated using Williamson-Hall equation:

$$\beta\cos\theta = k\lambda/\mathrm{D} + 4\varepsilon\sin\theta \quad (1)$$

where β is the observed FWHM, θ is the Bragg angle, *k* is the Scherer's constant, λ is the wavelength of the X-ray used, D is the crystallite size, ε is the strain present in the crystal. The observed results are shown in table 3. The crystalline size increases from 29.4 nm to 47.6 nm with annealing temperature, which may be due to the faster movement of molecules accelerating the solid reaction with the increase of annealing temperature[22].

The observed crystallite size is smaller than that reported by others [2,13].

3.2 morphology

Fig. 2 shows the SEM micrographs of $Li_{0.35}Ni_{0.3}Fe_{2.35}O_4$ powders with different annealing temperature. The particle size of sample annealed at 500 ℃ is obviously smaller than that of the sample annealed at 850 ℃. So, the particle size increases with annealing temperature. The ferrite samples annealed below 800 ℃ are the spherical aggregates and the sample annealed at 850 ℃ gradually show irregular hexagon. These indicate that the microstructures of the samples can be easily controlled by annealing temperature.

3.3 FT-IR studies

Fig. 3 depicts the FT-IR spectra of $Li_{0.35}Ni_{0.3}Fe_{2.35}O_4$ ferrite annealed at 500 - 850℃ in the spectral region 375 - 900 cm^{-1}. The absorption bands for synthesized ferrites with different annealing temperatures are given in Table 4. The exhibited three vibration bands of all samples can be ascribed to tetrahedral (T_d) and Octahedral (O_h) coordination compounds [23]. Absorption band v_1 is characteristic for the stretching of tetrahedral metal ion and oxygen bond, and v_2 is characteristic for the vibrations of oxygen in the direction perpendicular to the axis joining the tetrahedral ion and oxygen, which indicate the formation of spinel ferrite structure[24]. Absorption band v_3 is attributed to the Li^+ - O^{2-} complexes at octahedral site[23]. It is reported that the frequencies of the vibrations depend on cation oxygen bonding, lattice parameters and cation mass[25]. The shift of absorption peak position lead by the increasing annealed temperature indicate the change in the bond length of cation and oxygen ion at the tetrahedral and octahedral sites.

3.4 Magnetic measurements

The magnetic hysteresis loops of $Li_{0.35}Ni_{0.3}Fe_{2.35}O_4$ ferrites annealed at different temperatures are shown in Fig. 4. Table 5 shows the observed magnetic parameters such as saturation magnetization (M_s), remanence magnetization (M_r) and coercivity (H_c) etc. Generally, soft magnetic behaviors are shown in all samples and the magnetic hysteresis loops become narrower and longer with increasing annealing temperature as can be seen from the inset of Fig. 4. The variation in lattice parameters and saturation magnetization as function of annealing temperature is presented in Fig. 5. It is clearly seen that the

variation of saturation magnetization is irregular. However, the changes in behavior of lattice parameters and saturation magnetization with annealing temperature are almost similar. It is well known that magnetization of the samples can be explained on the basis of cation distribution and Neel's model. According to this model, the A-B super-exchange interaction is predominant over B-B and A-A exchange interactions. For the spinel ferrites the cations in tetrahedral (A site) and octahedral sublattices (B site) have opposite aligned magnetic moment, where the net magnetic moment defined as [26]

$$n_{th} = M_B - M_A \tag{2}$$

In the present study, the probable cation distribution can be written as

$$(Fe^{3+}{}_{(1-x-y)}Ni^{2+}{}_{x}Li^{1+}{}_{y})[Ni^{2+}{}_{0.3-x}Li^{1+}{}_{0.35-y}Fe^{3+}{}_{1.35+x+y}] \tag{3}$$

It is known that the Li^{+} is nonmagnetic in nature and does not contribute to the magnetization. Ni^{2+} and Fe^{3+} ions have magnetic moment of 2 μ_B and 5μ_B, respectively. Therefore, the net magnetic moment can be given by [26],

$$\mathrm{M}_B = 7.35 + 3x + 5y \tag{4}$$

$$M_A = 5 - 3x - 5y \tag{5}$$

$$n_{th} = M_B - M_A = 2.35 + 6x + 10y \tag{6}$$

It can be seen that the net magnetic moment increases with the increase of Li^{+} and Ni^{2+} contents in tetrahedron, which can be calculated from the compositions of ferrites with the ideal cation occupancy values observed by refinement XRD patterns. Furthermore, the experimental magnetic moment (n_B) can be expressed as:

$$n_B = [\, M_w \times M_s \,]/5585 \tag{7}$$

where M_W is the molecular weight of the sample, M_s is the saturation magnetization of sample and 5585 is magnetic factor [11]. According to the observed magnetic moment, the Yafet-Kittel (Y-K) angles can be calculated by the formula as follow:

$$n_B = M_B cos\alpha_{Y-K} - M_A \tag{8}$$

The values of theoretical magnetic moment (n_{th}), experimental magnetic moment (n_B), and Y-K angle are shown in table 5. It is evident that there are similar trends between

theoretical magnetic moment (n_{th}) and saturation magnetization (M_s) with annealing temperature below 800 ℃, which illustrate that the change of M_s can be ascribed to the cation distribution in tetrahedron and octahedron. The abnormal M_s for the sample annealed at 850 ℃ can be attributed to the larger Y-K angle. The larger Y-K angle of magnetic ions shows the decrease in the overlap of the wave functions between the two nearest neighboring magnetic ions and also between the magnetic ions and oxygen anions [13]. Therefore, the decrease in super exchange interactions between the magnetic ions and oxygen anions caused by the larger Y-K angle leads to a smaller M_s.

Fig. 6 shows the variation in average crystallite size (D) and coercivity (H_c) for $Li_{0.35}Ni_{0.3}Fe_{2.35}O_4$ ferrites as function of annealing temperature (T_a). The coercivity first increases and then decreases with the increase in crystallite size. It is well known that the change of H_c with the grain size can be explained on the basis of domain structure, critical diameter and the magneto-crystalline anisotropy. The value of the magneto-crystalline anisotropy was calculated by using the following relation:

$$K_1 = \frac{H_C \times M_S}{0.96} \tag{9}$$

The observed values are given in table 5. The change in the magneto-crystalline anisotropy constant can be attributed to the shape effect of the samples synthesized at different annealing temperature [11]. Furthermore, it is well known that in the single domain region, the coercivity increase with the particle size, which is attributed to the magnetic domain rotation. The highest coercivity of 115 Oe is observed at the annealing temperature of 600 ℃ with the grain size of 35.6 nm. However, the coercivity gradually decreases with annealing temperature increasing from 600 ℃ to 850 ℃, indicating multidomain nature for the sample annealing above 600 ℃, which is decided by domain wall displacement[14]. The ratio R of the remanence to the saturation magnetization (M_r/M_s) listed in Table 5 is derived from the hysteresis loops. The low value of R (below 0.2) also certifies the existence of multidomains in the ferrites. In present research, the coercivity reaches a maximum at 600 ℃ which can be considered as the critical size from single-domain to multi-domain transition behavior of the ferrites.

4. Conclusions

The $Li_{0.35}Ni_{0.3}Fe_{2.35}O_4$ ferrites have been synthesized with annealing temperature of 500 ℃, 600 ℃, 700 ℃, 800 ℃ and 850 ℃ using the sol-gel auto-combustion technique. Rietveld analysis of XRD data showed the structural transition from the α-spinel (*Fd*-3*m*) to β-spinel ($P4_332$) structure with the annealing temperature increasing, from which the ideal cation occupation of ferrites was also observed. The goodness of fit values indicated the goodness of refinement of diffraction data for ferrites. Three characteristic FTIR absorption bands confirmed the formation of tetrahedral (T_d) and Octahedral (O_h) coordination compounds including Li^+-O^{2-} complexes. The magnetic hysteresis loops become narrower and longer with higher saturation magnetization and lower coercivity, which indicated that the ferrites have better soft magnetic properties with increase of annealing temperature. The change of saturation magnetization is almost similar to that of lattice parameters, which verified the correctness of the occupation of cations. The coercivity initially increased and then decreased with the increase of crystallite size, which demonstrated that the 600℃-annealed grain size is close to transition grain size from single to multidomain region.

Acknowledgement

This work was supported by National Natural Science Foundation of China (under Grant No. 51271130).

References:

[1] Z. A. Gilani, M. S. Shifa, H. M. N. ul H. K. Asghar, M. A. Khan, M. N. Anjum, M. N. Usmani, R. Ali, and M. F. Warsi, Ceram. Int. **44**, 1881 (2018).

[2] M. F. Warsi, Z. A. Gilani, N. F. Al-Khalli, M. Sarfraz, M. A. Khan, M. N. Anjum, and I. Shakir, Ceram. Int. **43**, 14807 (2017).

[3] M. A. Islam, M. Hasan, and A. K. M. A. Hossain, J. Magn. Magn. Mater. **424**, 108 (2017).

[4] R. G. Kharabe, S. A. Jadhav, A. M. Shaikh, D. R. Patil, and B. K. Chougule, Mater. Chem. Phys. **72**, 77 (2001).

[5] A. A. Momin, R. Parvin, and A. K. M. A. Hossain, J. Magn. Magn. Mater. **423**, 124 (2017).

[6] R. G. Kharabe, R. S. Devan, and B. K. Chougule, J. Alloy. Compd. **463**, 67 (2008).

[7] I. Ahmad, T. Abbas, A. B. Ziya, and A. Maqsood, Ceram. Int. **40**, 7941 (2014).

[8] M. Srivastava, S. Layek, J. Singh, A. K. Das, H. C. Verma, A. K. Ojha, N. H. Kim, and J. H. Lee, J. Alloy. Compd. **591**, 174 (2014).

[9] M. F. Al-Hilli, S. Li, and K. S. Kassim, Mater. Sci. Eng. B-Adv. Funct. Solid-State Mater. **158**, 1 (2009).

[10] G. Aravind, M. Raghasudha, D. Ravinder, M. M. Raja, S. S. Meena, P. Bhatt, and M. Hashim, Ceram. Int. **42**, 2941 (2016).

[11] R. P. Patil, P. P. Hankare, K. M. Garadkar, and R. Sasikala, J. Alloy. Compd. **523**, 66 (2012).

[12] N. Singh, A. Agarwal, and S. Sanghi, J. Alloy. Compd. **509**, 7543 (2011).

[13] J. Jiang, Y.-M. Yang, and L.-C. Li, J. Alloy. Compd. **464**, 370 (2008).

[14] E. K. Al-Shakarchi, S. H. Lafta, A. M. Musa, M. Farle, and R. Salikov, J. Supercond. Nov. Magn **29**, 923 (2016).

[15] M. F. Al Hilli, S. Li, and K. S. Kassim, Mater. Chem. Phys. **128**, 127 (2011).

[16] S. Sutradhar, S. Pati, S. Acharya, S. Das, D. Das, and P. K. Chakrabarti, J. Magn. Magn. Mater. **324**, 1317 (2012).

[17] Z. Noreen, I. Ahmad, F. Siddiqui, A. B. Ziya, T. Abbas, and H. Bokhari, Ceram. Int. **43**, 10784 (2017).

[18] D. Ridgley, H. Lessoff, and J. Childress, J. Am. Ceram. Soc. **53**, 304 (1970).

[19] M. A. Islam, M. Hasan, and A. K. M. A. Hossain, J. Magn. Magn. Mater. **424**, 108 (2017).

[20] C. Kolekar, P. Kamble, and A. Vaingankar, J. Magn. Magn. Mater. **138**, 211 (1994).

[21] A. P. Surzhikov, A. V. Malyshev, E. N. Lysenko, V. A. Vlasov, and A. N. Sokolovskiy, Ceram. Int. **43**, 9778 (2017).

[22] S. C. Watawe, B. D. Sutar, B. D. Sarwade, and B. K. Chougule, Int. J. Inorg. Mater. **3**, 819 (2001).

[23] P. Thakur, R. Sharma, V. Sharma, and P. Sharma, Mater. Chem. Phys. **193**, 285 (2017).

[24] D. Ravinder, Mater. Lett. **40**, 205 (1999).

[25] A. A. Al-Ghamdi, F. S. Al-Hazmi, L. S. Memesh, F. S. Shokr, and L. M. Bronstein,

J. Alloy. Compd. **712**, 82 (2017).

[26] P. Gao, X. Hua, V. Degirmenci, D. Rooney, M. Khraisheh, R. Pollard, R. M. Bowmand, and E. V. Rebrov, J. Magn. Magn. Mater. **348**, 44 (2013).

Figure captions

Fig. 1. Rietveld refined X-ray diffraction patterns of $Li_{0.35}Ni_{0.3}Fe_{2.35}O_4$ soft ferrites annealed at (a) 500 ℃, (b) 600℃, (c) 700℃, (d) 800℃ and (e) 850℃. red points: the experimental data, black lines: the calculated pattern, blue ticks: Bragg position, green lines: the difference between the experimental and the refined curves.

Fig. 2. Micrographs for $Li_{0.35}Ni_{0.3}Fe_{2.35}O_4$ soft ferrites annealed at (a) 500 ℃ (b) 600 ℃ (c) 700 ℃ (d) 800 ℃ (e) 850 ℃.

Fig. 3. FT-IR spectra for $Li_{0.35}Ni_{0.3}Fe_{2.35}O_4$ ferrites annealed at 500 - 850 ℃.

Fig. 4. Magnetic hysteresis loop for $Li_{0.35}Ni_{0.3}Fe_{2.35}O_4$ ferrites annealed at 500-850 ℃ and the inset is showing the magnified view.

Fig. 5. Variation in lattice parameters (a) and saturation magnetization (M_s) for $Li_{0.35}Ni_{0.3}Fe_{2.35}O_4$ ferrites as function of annealing temperature (T_a).

Fig. 6. Variation in average crystallite size (D) and coercivity (H_c) for $Li_{0.35}Ni_{0.3}Fe_{2.35}O_4$ ferrites as function of annealing temperature (T_a).

Table 1. The agreement factors R_p, R_{wp}, R_{exp} and χ^2 after the Rietveld refinement of XRD data for $Li_{0.35}Ni_{0.3}Fe_{2.35}O_4$ soft ferrites.

Table 2. Structural parameters for $Li_{0.35}Ni_{0.3}Fe_{2.35}O_4$ ferrites annealed at 500 ℃ and 600 ℃ from the Rietveld refinement in $P4_332$ space group.

Table 3. The lattice parameter ($a_{x\text{-}ray}$) and average crystalline size (D) of $Li_{0.35}Ni_{0.3}Fe_{2.35}O_4$ ferrites with different annealing temperatures. The compositions of ferrites are listed with the ideal cation occupancy values.

Table 4. Fundamental vibrational frequency bands of $Li_{0.35}Ni_{0.3}Fe_{2.35}O_4$ ferrites.

Table 5. Saturation magnetization (M_s), remanence magnetization (M_r), coercivity (H_c), experimental magnetic moment (n_B), theoretical magnetic moment (n_{th}), R (M_r/M_s), magneto-crystalline anisotropy constant (K_1) and Yafet-Kittel angles (Y-K) of the $Li_{0.35}Ni_{0.3}Fe_{2.35}O_4$ ferrite as function of annealing temperature (T_a).

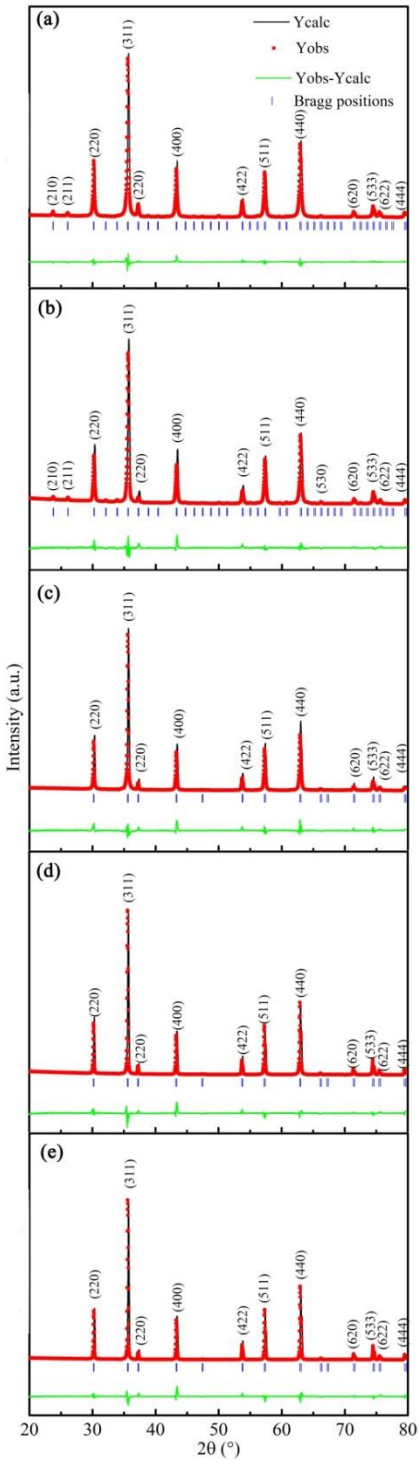

Fig. 1. Rietveld refined X-ray diffraction patterns of $Li_{0.35}Ni_{0.3}Fe_{2.35}O_4$ soft ferrites annealed at (a) 500 ℃, (b) 600℃, (c) 700℃, (d) 800℃ and (e) 850℃. red points: the experimental data, black lines: the calculated pattern, blue ticks: Bragg position, green lines: the difference between the experimental and the refined curves. (For interpretation of the references to color in this figure legend, the reader is referred to the Web version of this article.)

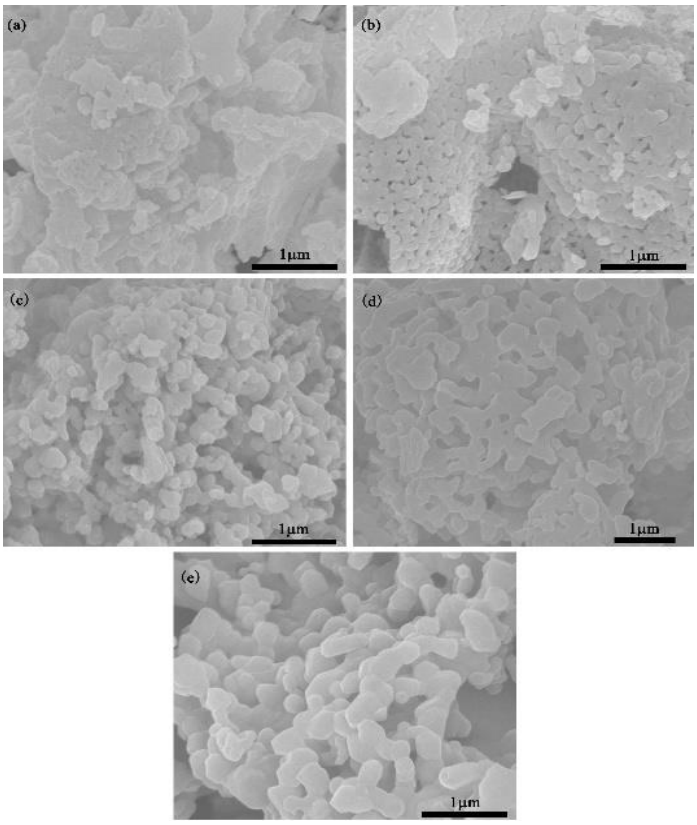

Fig. 2. Micrographs for $Li_{0.35}Ni_{0.3}Fe_{2.35}O_4$ soft ferrites annealed at (a) 500 ℃ (b) 600 ℃ (c) 700 ℃ (d) 800 ℃ (e) 850 ℃.

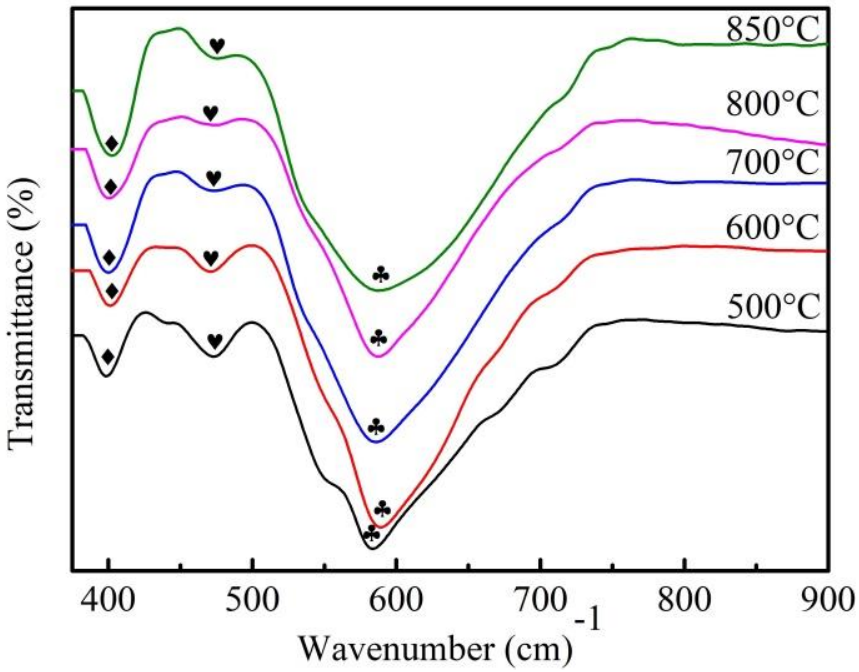

Fig. 3. FT-IR spectra for $Li_{0.35}Ni_{0.3}Fe_{2.35}O_4$ ferrites annealed at 500 - 850 ℃.

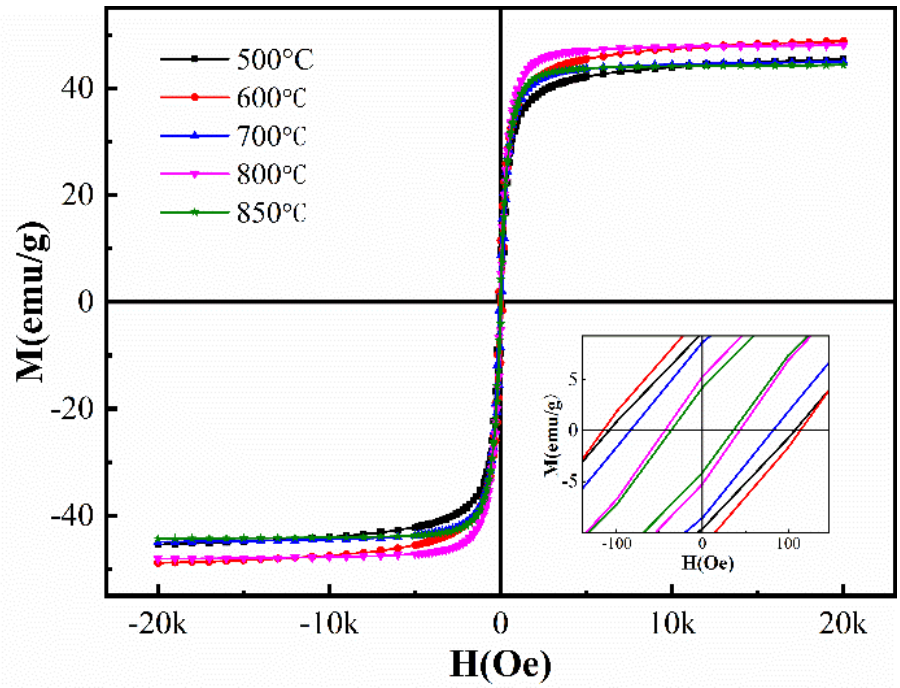

Fig. 4. Magnetic hysteresis loop for $Li_{0.35}Ni_{0.3}Fe_{2.35}O_4$ ferrites annealed at 500-850 °C and the inset is showing the magnified view.

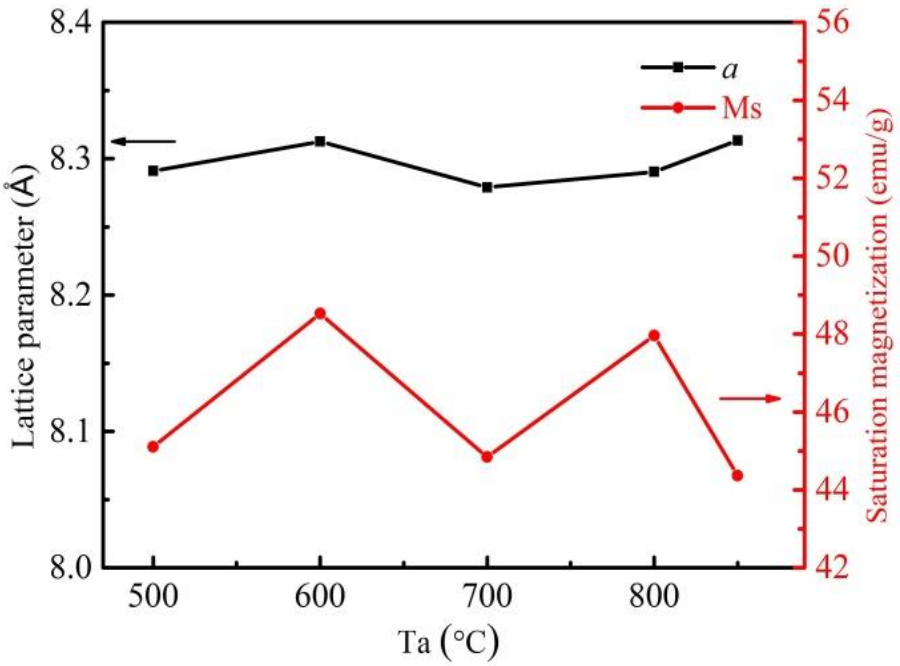

Fig. 5. Variation in lattice parameters (a) and saturation magnetization (M_s) for $Li_{0.35}Ni_{0.3}Fe_{2.35}O_4$ ferrites as function of annealing temperature (T_a).

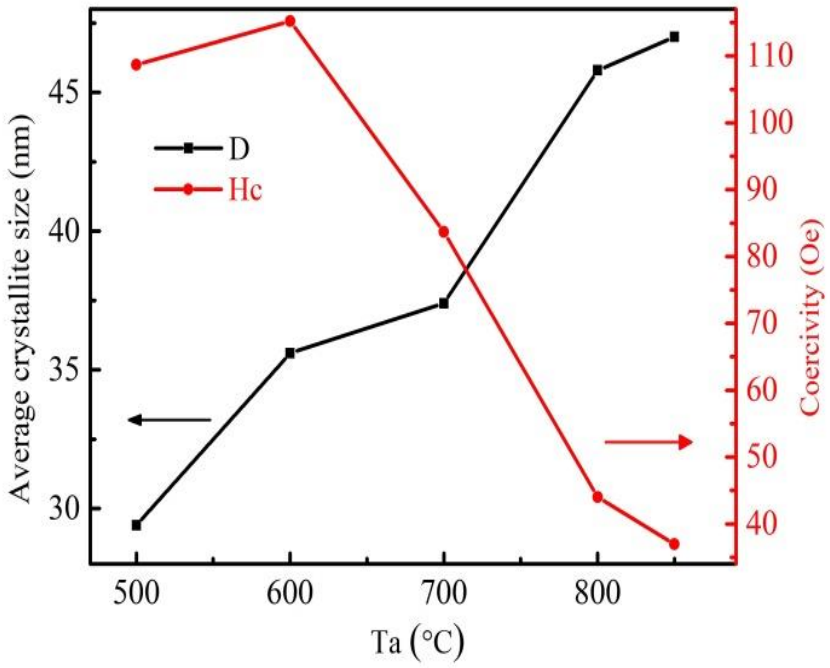

Fig. 6. Variation in average crystallite size (D) and coercivity (H_c) for $Li_{0.35}Ni_{0.3}Fe_{2.35}O_4$ ferrites as function of annealing temperature (T_a).

Table 1

The agreement factors R_p, R_{wp}, R_{exp} and χ^2 after the Rietveld refinement of XRD data for $Li_{0.35}Ni_{0.3}Fe_{2.35}O_4$ soft ferrites.

Ta (°C)	Rietveld parameters			
	R_p	R_{wp}	R_{exp}	χ^2
500 °C	10.9	13.4	9.24	1.45
600 °C	19.1	19.9	9.37	2.13
700 °C	21.3	22.9	10.48	2.18
800 °C	19.9	21.7	10.03	2.16
850 °C	17.9	21.2	9.47	2.23

Table 2

Structural parameters for $Li_{0.35}Ni_{0.3}Fe_{2.35}O_4$ ferrites annealed at 500 ℃ and 600 ℃ from the Rietveld refinement in $P4_332$ space group.

Atom	Site	Coordinates			Occupancy determined for sample	
		x	y	z	500 ℃	600 ℃
Li(1)	4b	0.625	0.625	0.625	0.35	0.35
Ni(1)	4b	0.625	0.625	0.625	0.15	0.01
Fe(1)	12d	0.125	0.3661	0.8839	1.35	1.41
Ni(2)	12d	0.125	0.3661	0.8839	0.15	0.23
Fe(2)	8c	-0.0036	-0.0036	-0.0036	1.0	0.94
Ni(3)	8c	-0.0036	-0.0036	-0.0036	-	0.06
O(1)	8c	0.3869	0.3869	0.3869	-	-
O(2)	24e	0.1177	0.1268	0.3806	-	-

Table 3

The lattice parameter ($a_{x\text{-}ray}$) and average crystalline size (D) of $Li_{0.35}Ni_{0.3}Fe_{2.35}O_4$ ferrites with different annealing temperatures. The compositions of ferrites are listed with the ideal cation occupancy values.

Ta (℃)	composition	$a_{x\text{-}ray}$ (Å)	D (nm)
500 ℃	$(Fe_{1.0})[Ni_{0.3}Li_{0.35}Fe_{1.35}]O_4$	8.2910	29.4
600 ℃	$(Ni_{0.06}Fe_{0.94})[Ni_{0.24}Li_{0.35}Fe_{1.41}]O_4$	8.3126	35.6
700 ℃	$(Fe_{1.0})[Ni_{0.3}Li_{0.35}Fe_{1.35}]O_4$	8.2790	37.4
800 ℃	$(Ni_{0.1}Li_{0.05}Fe_{0.85})[Ni_{0.2}Li_{0.3}Fe_{1.5}]O_4$	8.2903	45.8
850 ℃	$(Ni_{0.1}Li_{0.1}Fe_{0.8})[Ni_{0.2}Li_{0.25}Fe_{1.55}]O_4$	8.3134	47.6

Table 4

Fundamental vibrational frequency bands of $Li_{0.35}Ni_{0.3}Fe_{2.35}O_4$ ferrites.

Ta (℃)	ν_1 (cm^{-1})	ν_2 (cm^{-1})	ν_3 (cm^{-1})
500	583	398	473
600	590	402	471
700	586	401	474
800	588	401	475
850	587	402	475

Table 5

Saturation magnetization (M_s), remanence magnetization (M_r), coercivity (H_c), experimental magnetic moment (n_B), theoretical magnetic moment (n_{th}), R (M_r/M_s), magneto-crystalline anisotropy constant (K_1) and Yafet-Kittel angles (Y-K) of the $Li_{0.35}Ni_{0.3}Fe_{2.35}O_4$ ferrite as function of annealing temperature (T_a).

Ta (°C)	M_s (emu/g)	M_r (emu/g)	H_c (Oe)	n_B (μ_B)	n_{th} (μ_B)	R=Mr/Ms	K_1 (erg/m^3)	Y-K angle (°)
500	45.11	9.66	109	1.36	2.35	0.21	5002	30.15
600	48.52	11.49	115	1.46	2.71	0.24	5704	33.51
700	44.84	8.64	84	1.35	2.35	0.19	3829	30.27
800	47.96	5.28	44	1.44	3.45	0.11	2154	41.78
850	44.37	4.16	37	1.33	3.95	0.09	1673	47.24

Figures

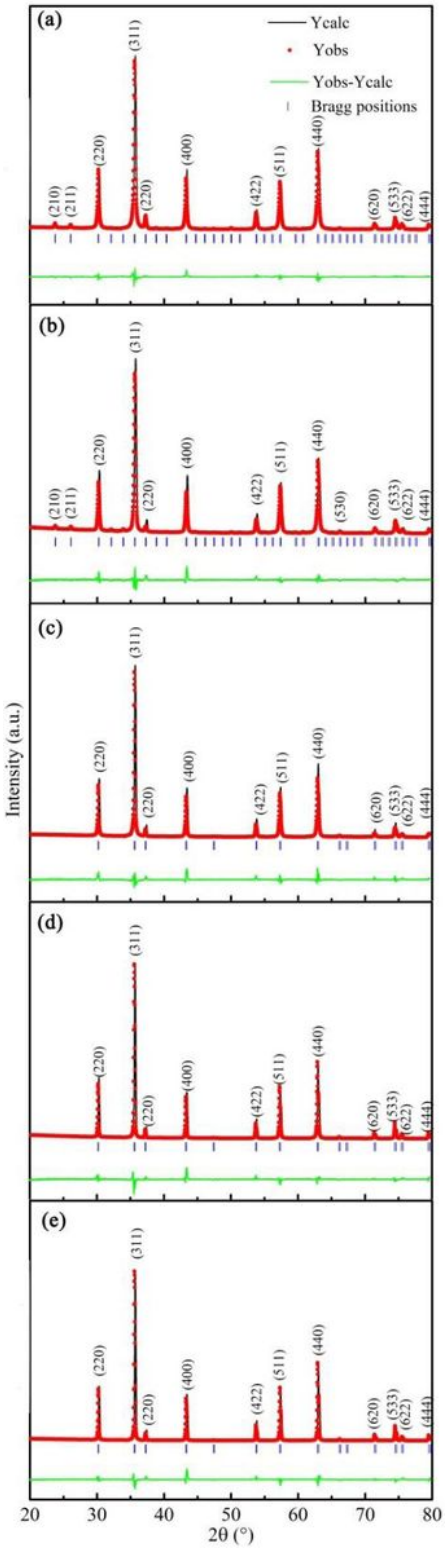

Figure 1

Rietveld refined X-ray diffraction patterns of Li0.35Ni0.3Fe2.35O4 soft ferrites annealed at (a) 500 ℃, (b) 600℃, (c) 700℃, (d) 800℃ and (e) 850℃. red points: the experimental data, black lines: the calculated pattern, blue ticks: Bragg position, green lines: the difference between the experimental and the refined curves.

(For interpretation of the references to color in this figure legend, the reader is referred to the Web version of this article.)

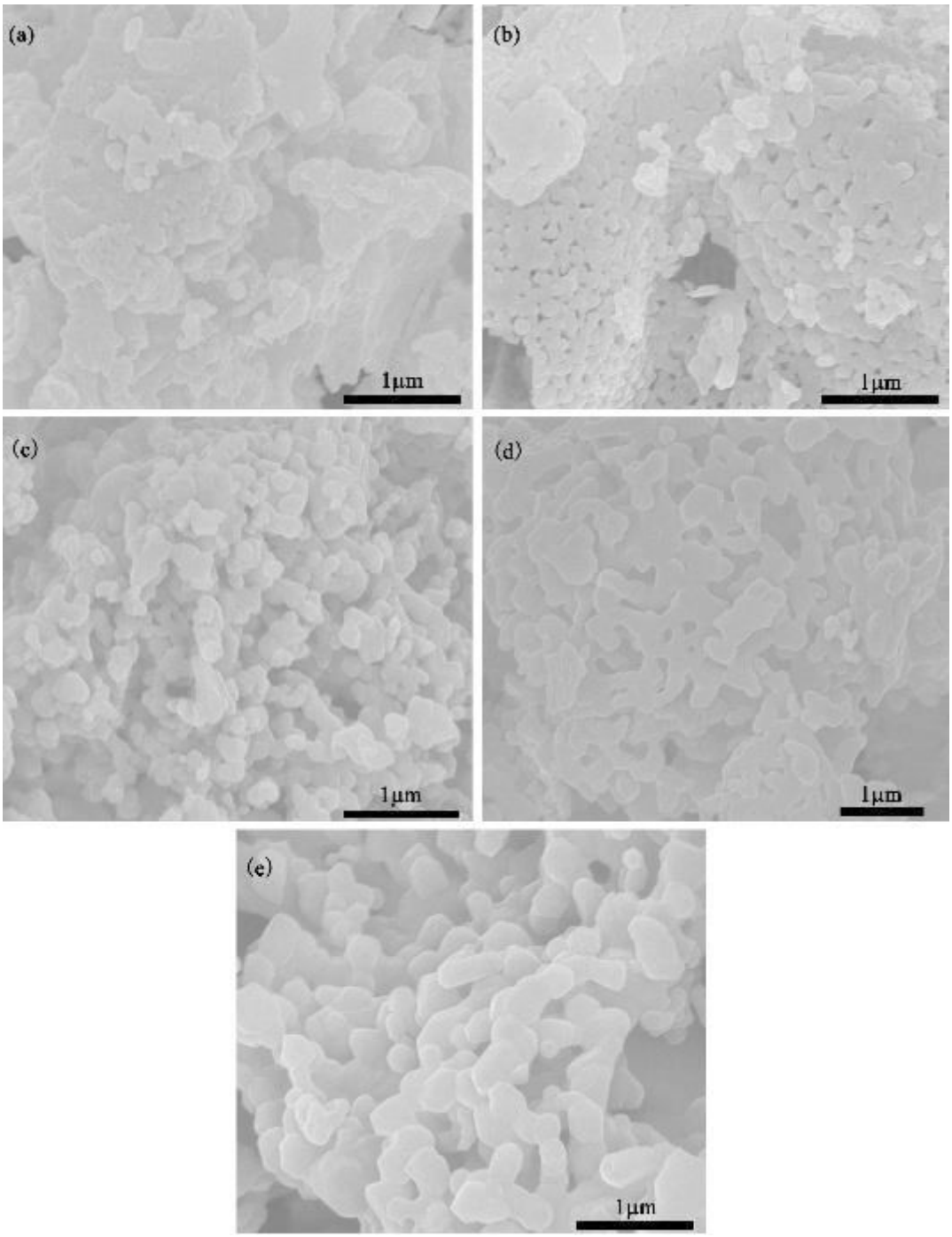

Figure 2

Micrographs for Li0.35Ni0.3Fe2.35O4 soft ferrites annealed at (a) 500 □ (b) 600 □ (c) 700 □ (d) 800 □ (e) 850 □.

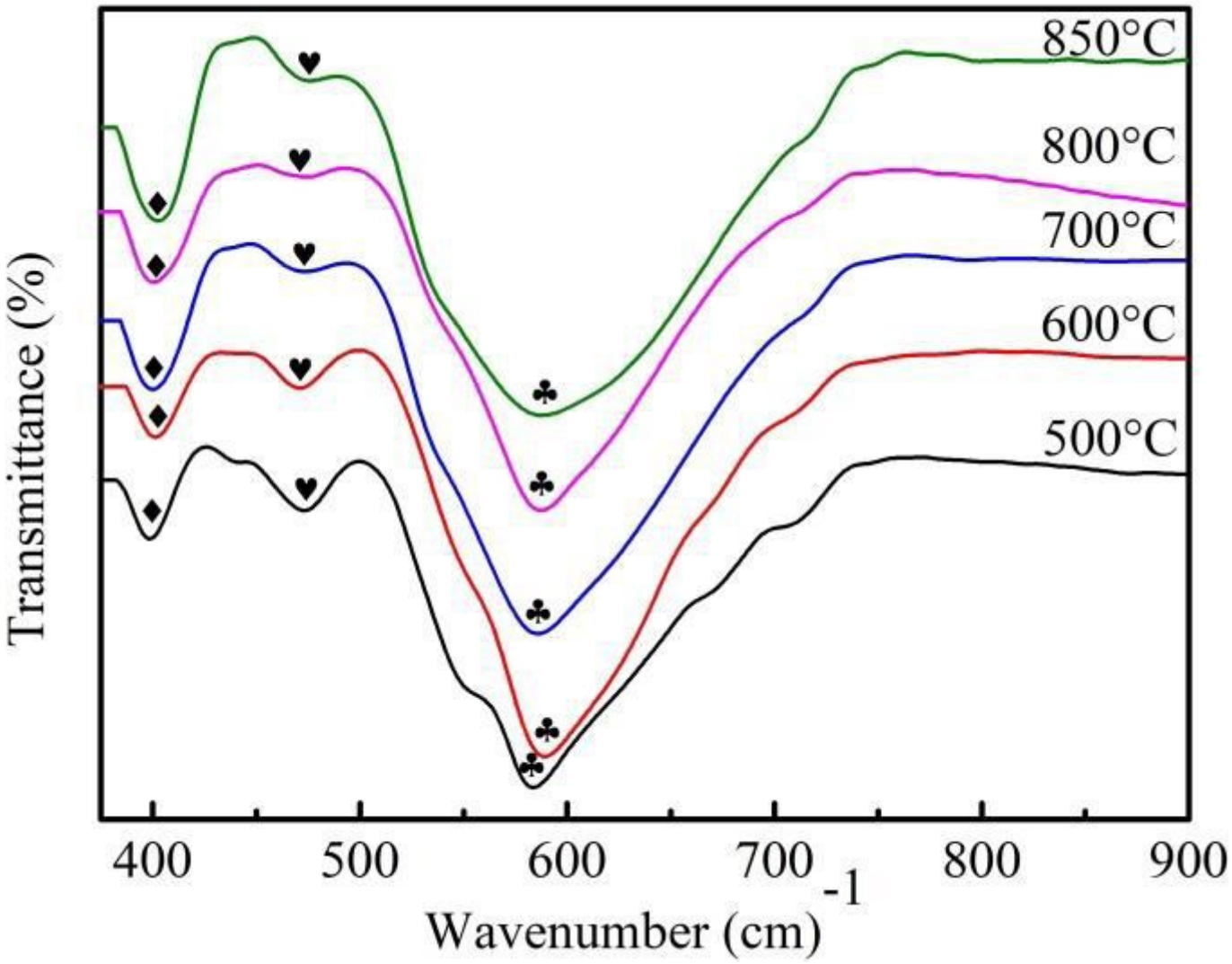

Figure 3

FT-IR spectra for Li0.35Ni0.3Fe2.35O4 ferrites annealed at 500 - 850 ℃.

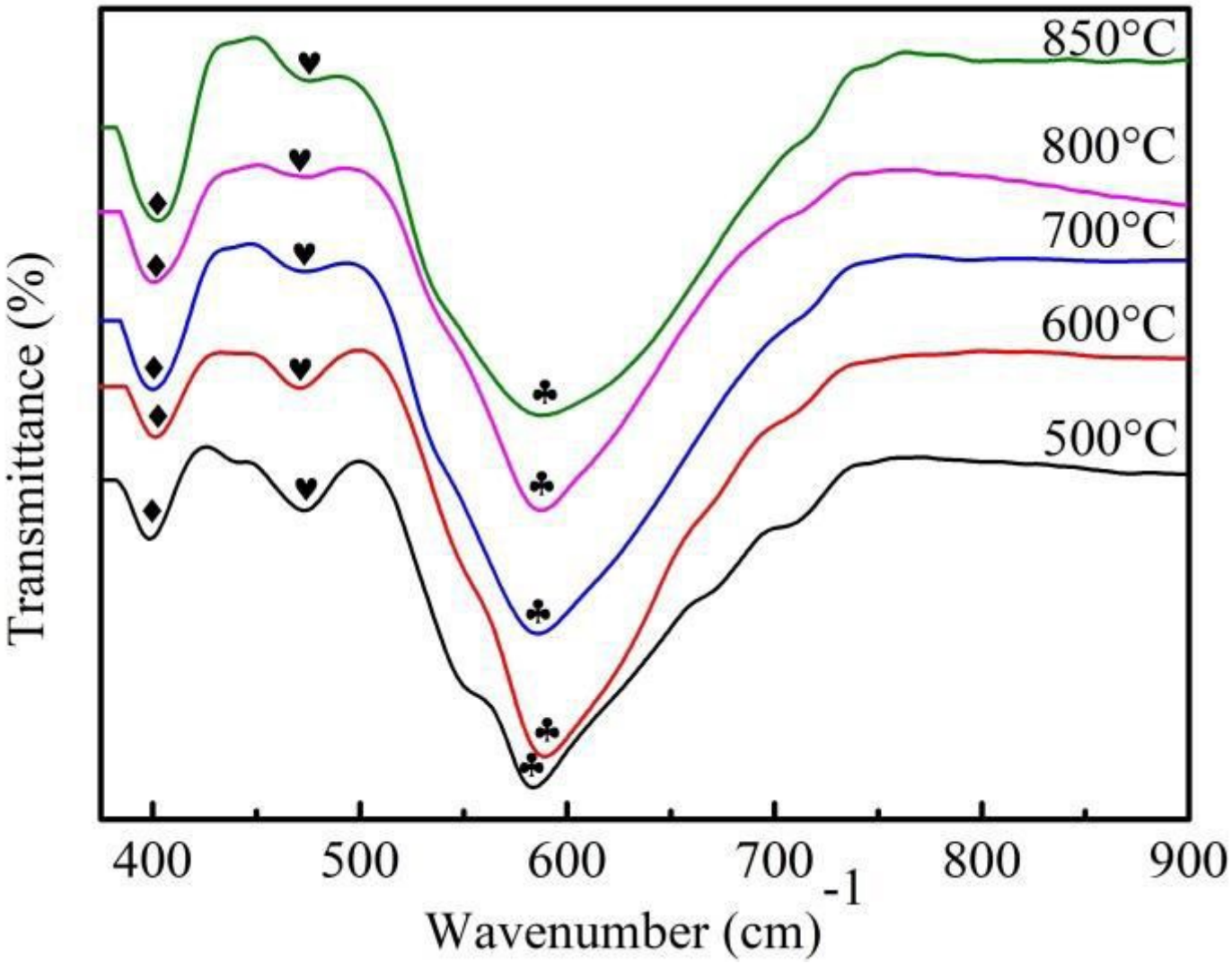

Figure 4

Magnetic hysteresis loop for Li0.35Ni0.3Fe2.35O4 ferrites annealed at 500-850 □ and the inset is showing the magnified view.

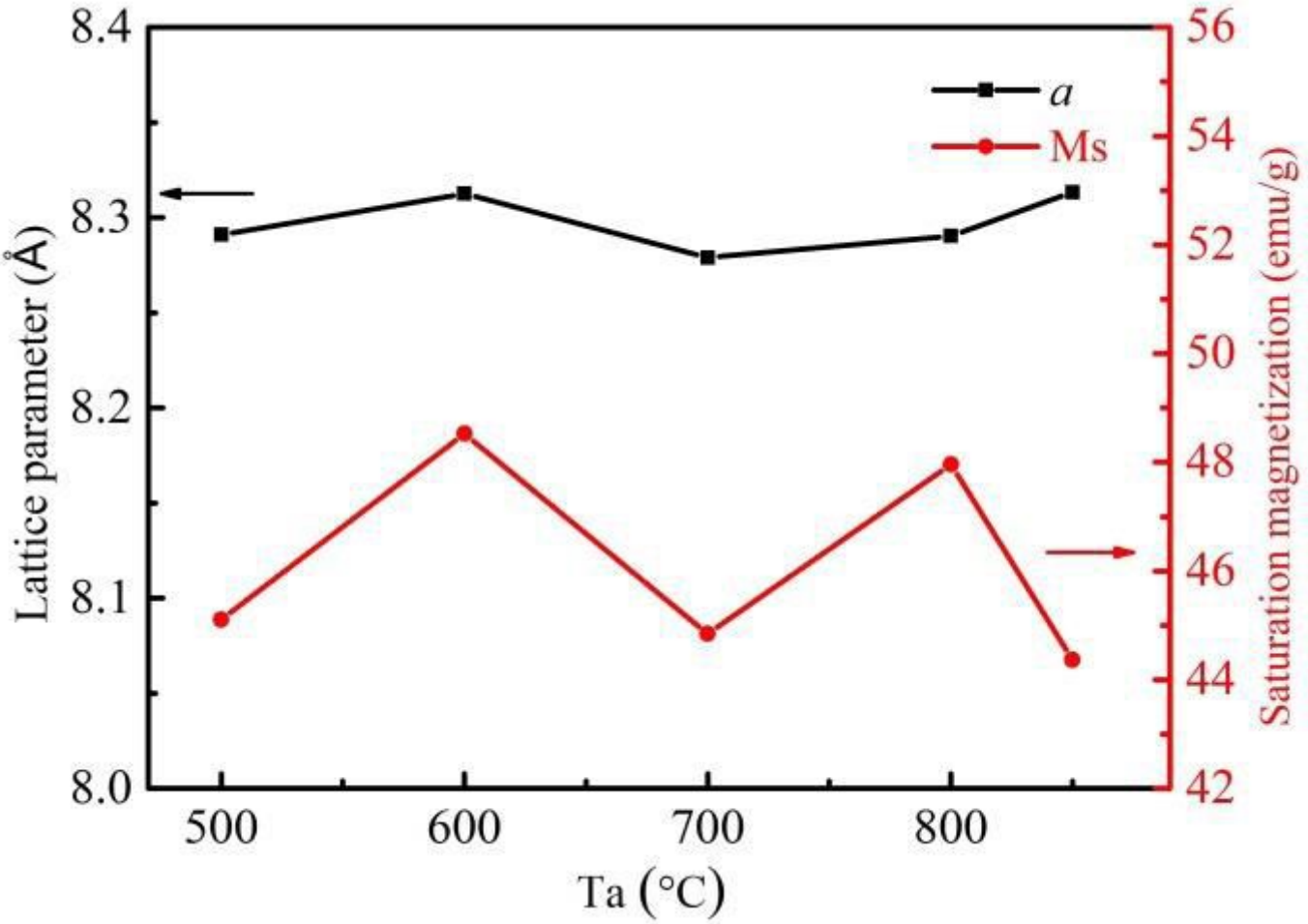

Figure 5

Variation in lattice parameters (a) and saturation magnetization (Ms) for Li0.35Ni0.3Fe2.35O4 ferrites as function of annealing temperature (Ta).

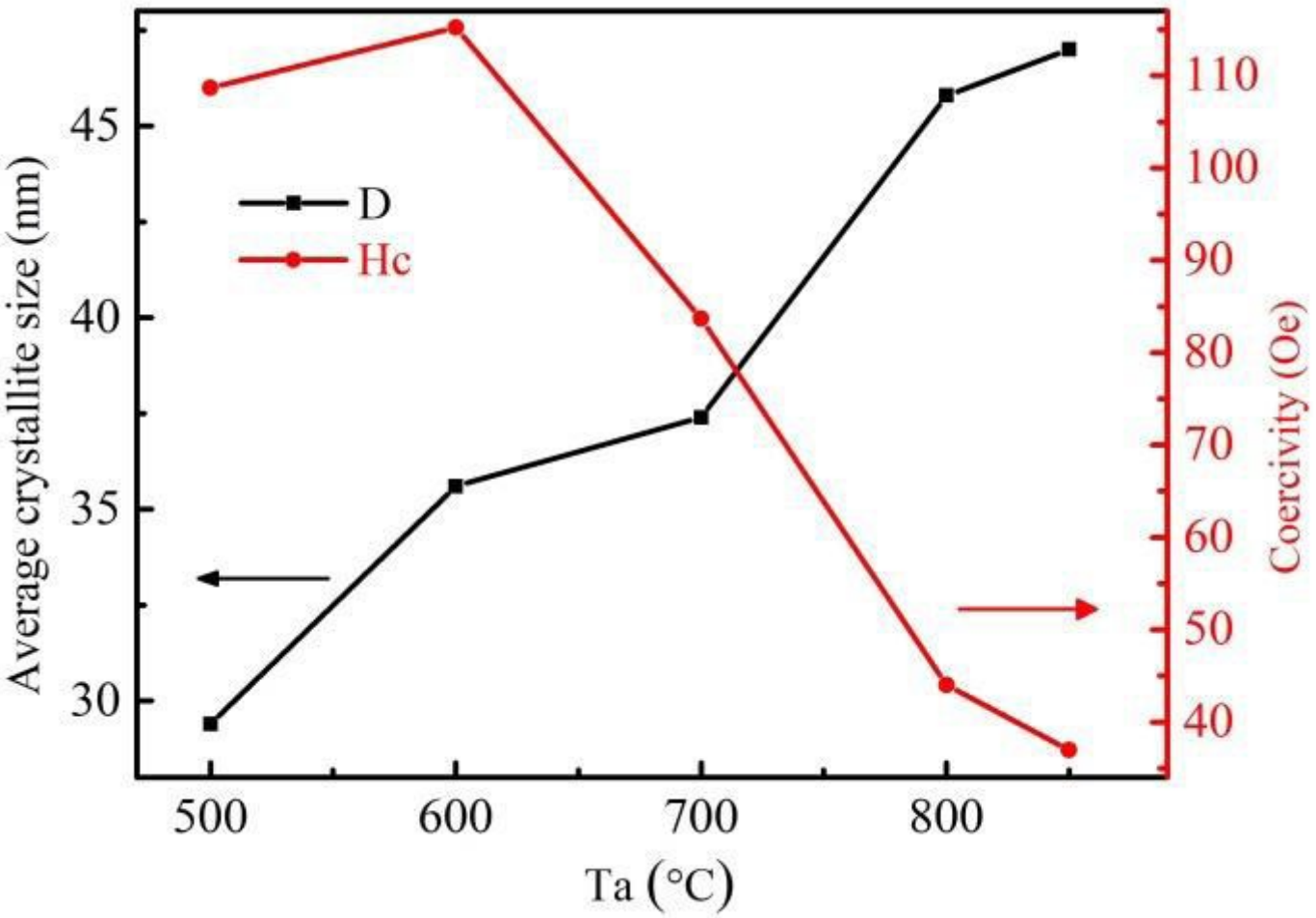

Figure 6

Variation in average crystallite size (D) and coercivity (Hc) for Li0.35Ni0.3Fe2.35O4 ferrites as function of annealing temperature (Ta).